Advances in Water Resources 125 (2019) 57–67

Contents lists available at ScienceDirect

Advances in Water Resources

journal homepage: www.elsevier.com/locate/advwatres

A Dual Domain stochastic lagrangian model for predicting transport in open channels with hyporheic exchange

Thomas Sherman[a,*], Kevin R. Roche[a], David H. Richter[a], Aaron I. Packman[b], Diogo Bolster[a]

[a] Department of Civil & Environmental Engineering & Earth Sciences, University of Notre Dame, 46556 IN, USA
[b] Department of Civil and Environmental Engineering, Northwestern University, Evanston, IL 60208, USA

ARTICLE INFO

Keywords:
Hyporheic exchange
Transport
CTRW
Direct numerical simulation

ABSTRACT

The exchange of surface and subsurface waters plays an important role in understanding and predicting large scale transport processes in streams and rivers. Accurately capturing the influence of small-scale features associated with turbulent dispersion on exchange in an upscaled framework is necessary for developing reliable predictive models at the reach scale. In this work, we use high-fidelity direct numerical simulations (DNS) to fully resolve turbulent flow and hyporheic exchange in an open channel. We parameterize a 2D particle tracking model with the average DNS velocity and scalar diffusivity profiles. Breakthrough curves and rate of surface mass loss to the subsurface in both models agree after a sufficient distance downstream from particle injection. Finally we find that the travel time/distance joint pdf contains enough information to parameterize a 1D dual domain coupled Continuous Time Random Walk (ddc-CTRW) model that successfully reproduces the behavior of both the DNS and the 2D particle tracking model, allowing accurate prediction of breakthrough curves. Predicting breakthrough curves with a fully parameterized ddc-CTRW reduces cpu time by orders of magnitude when compared with DNS.

1. Introduction

Streams and rivers play a fundamental role in transporting minerals, nutrients, and other solutes across local to continental scales, thereby integrating the biological, chemical, and geologic processes of watersheds (Battin et al., 2009; Boano et al., 2014; Gooseff, 2010). Modeling transport of these materials in river systems is especially challenging because the physical processes controlling macro-scale transport range from the sediment to the stream reach scale and resolving all of these scales is far too costly. Of particular significance is the interaction of fast moving surface waters with underlying slow hyporheic flow, which delays downstream transport and enhances biological processing of nutrients (Boano et al., 2014; Wörman et al., 2002). This exchange of water across the sediment-water interface (SWI) into and out of the hyporheic zone (the subsurface region penetrated by surface waters) must be captured in upscaled modeling frameworks if we hope to advance predictive transport models at the stream reach scale and above.

Classical open-channel flow theory assumes an impermeable boundary at the SWI, allowing one to treat transport in rivers as a Fickian process described with an advection-dispersion equation (ADE), as first derived by G.I. Taylor in (Taylor, 1954). However, decades of experimental observations in rivers and streams show that this assumption is consistently violated (Aubeneau et al., 2014; González-Pinzón et al., 2013; Haggerty et al., 2000; Harvey et al., 1996). In reality, solutes in the water column and hyporehic zone are mixed by molecular diffusion and mechanical/turbulent dispersion (Voermans et al., 2018). Due to such exchange, solute is retained in the slower-moving pore waters for long time-scales, leading to large-scale anomalous transport, which is transport that cannot be described with a traditional one-dimensional Fickian ADE model (Aubeneau et al., 2014; Benson et al., 2001; Haggerty et al., 2001). In field-scale conservative tracer experiments, observed breakthrough curves (BTCs), which measure the temporal evolution of in-stream solute concentration, display anomalous transport as persistent power law tailing behavior, resulting in an elevated concentration at late times relative to an ADE prediction (Haggerty et al., 2002). Additionally, measured BTCs can exhibit an apparent mass loss to the subsurface (Wlostowski et al., 2016), suggesting solute remains in the sediment bed for timescales that far exceed those in the surface channel.

Among other state-of-the-art modeling approaches, Continuous Time Random Walks (CTRW), have been shown to sufficiently describe anomalous transport in a broad range of hydrologic systems (Berkowitz et al., 2006; Berkowitz and Scher, 2009; Cortis and Birkholzer, 2008). In a CTRW framework, a solute plume is conceptualized as an infinite number of particles that jump through time and space with spatial and temporal increments l and τ, respectively, sampled from a distribution $\Psi(l, \tau)$. Particle travel times and distances are often assumed to be decoupled and successive jumps uncorrelated (Berkowitz et al., 2006). In

* Corresponding author.
E-mail address: tsherma3@nd.edu (T. Sherman).

https://doi.org/10.1016/j.advwatres.2019.01.007
Received 26 June 2018; Received in revised form 10 January 2019; Accepted 11 January 2019
Available online 15 January 2019
0309-1708/

systems that demonstrate strong velocity correlations, the uncorrelated assumption can be relaxed, and an additional correlation parameter can be included to capture persistent behavior (Bolster et al., 2014; Borgne et al., 2008; Kang et al., 2014; Sherman et al., 2017). The CTRW framework was first applied to river systems in Boano et al. (2007), where they investigated the effects of residence time distribution in the hyporheic zone on BTCs. As applied in their framework, particle travel times and distances are assumed independent (i.e. uncoupled), $\Psi(l,t) = \lambda(l)\psi(t)$, where $\lambda(l)$ is a jump-length distribution and $\psi(t)$ is a wait-time distribution. Particles only move when in the water column, meaning subsurface longitudinal travel distances are assumed to be insignificant relative to travel distances in the stream. The model has been used to successfully describe both solute and fine particle transport in streams Drummond et al. (2014); Stonedahl et al. (2012). However, the uncoupled assumption may not reflect universal behaviors, as high streamwise velocities in highly permeable beds can allow particles to travel significant distances in the subsurface (Roche et al., 2018).

To overcome this possible limitation we propose a dual domain coupled CTRW (ddc-CTRW) model that generalizes previously applied CTRW models by relaxing the independence requirement. In this framework, solute is conceptualized as a large number of particles, but now particle trajectories consist of alternating jumps between the surface and subsurface domains and are sampled from different joint probability density functions for each domain. Two major benefits of such an approach are i) all particles travel at a realistic velocity because time and distance are coupled, and ii) accounting for streamwise particle fluxes in the hyporehic zone allows a particle's first passage across a plane to occur while in the subsurface. This causes an apparent surface mass loss that is observed in breakthrough curve measurements and cannot occur if the subsurface is considered as entirely immobile.

We compare BTC predictions from our ddc-CTRW upscaled model with results obtained from a high-fidelity turbulence resolving direct numerical simulation (DNS) (González et al., 2017; Park et al., 2018). We also parameterize a two dimensional, Lagrangian particle-tracking, open channel flow model (Aquino et al., 2015; Aubeneau et al., 2014; Li et al., 2017) from the spatio-temporally averaged DNS velocity and scalar diffusivity profiles, and track particle travel times and distances to create joint probabilty density distributions for the surface and subsurface domains. These pdfs act as inputs for our 1D ddc-CTRW framework, which allows us to make predictions of DNS measurements at significantly reduced computational cost. With this work we aim to answer the following questions: "Does an idealized, 2D particle tracking model faithfully portray transport in a fully turbulent system?" and "What statistics from the 2D model are required to accurately estimate DNS measurements with a 1D upscaled framework?"

2. Model frameworks

We model solute transport in an idealized stream with a 3D DNS, a 2D particle tracking simulation (henceforth referred to as the "2D model"), and the new 1D ddc-CTRW. Computational cost decreases from 3D to 1D, and so we investigate the statistics needed to properly reduce the full 3D flow simulation to a 1D downstream transport model. The stream reach is idealized as a straight, open channel with an underlying sediment bed exerting a uniform drag on the flow. The sediment bed has infinite depth, and subsurface flow approaches a Darcy velocity with increasing streambed depth (i.e. the average velocity when an applied pressure gradient balances sediment resistance). Solute is conceptualized as an ensemble of infinitesimal, massless particles that are simultaneously released from a point at the SWI.

2.1. 3D: Direct numerical simulation

To numerically model turbulent exchange between the surface and subsurface, we utilize DNS coupled with Lagrangian tracers in a system designed to mimic free stream, wall-bounded turbulence above a porous substrate. The DNS solves the Navier-Stokes equations for fluid mass and momentum conservation, and in the free stream resolves all scales of motion on the computational grid. The governing mass and momentum equations are given by

$$\nabla \cdot \mathbf{u} = 0, \tag{1}$$

$$\frac{\partial \mathbf{u}}{\partial t} + \mathbf{u} \cdot \nabla \mathbf{u} = -\frac{1}{\rho}\nabla p + \nu \nabla^2 \mathbf{u} + \mathbf{F}_{\mathbf{sed}}, \tag{2}$$

where $\mathbf{F}_{\mathbf{sed}}$ is a resistance force applied below $z = 0$ to mimic sediment:

$$\mathbf{F}_{\mathbf{sed}} = \begin{cases} 0 & z > 0 \\ -\frac{C_D}{H_{fs}}|\mathbf{u}|\mathbf{u} & z < 0. \end{cases} \tag{3}$$

Hence, the subsurface is considered as a continuum, similar to a Darcy model but with the drag coefficient representing flow resistance. Rather than directly resolving flow on the scale of individual sediment grains (i.e. between spaces in the porous media), we treat the subsurface as a continuous source of resistance for the flow, similarly to how vegetation canopies are represented in atmospheric boundary layer models (Finnigan et al., 2009). In this way, coupling between the turbulent surface flow and the subsurface is done continuously.

The incompressible flow solver uses a pseudospectral discretization in the horizontal directions x and y, and second-order finite differencing in the vertical. The code is well-established, routinely used for studying turbulent flow, and has been validated and tested for grid convergence (González et al., 2017; Richter and Sullivan, 2013; Sweet et al., 2018). In the vertical direction, grid stretching is used near $z = 0$ to resolve motions in the open channel near the SWI; i.e., the wall-normal grid spacing Δz is smaller near the SWI than in the upper free stream since vertical gradients are larger there. A computational mesh of size [128, 128, 128] is applied over domain lengths of $[2\pi, \pi, 1.6]H_{fs}$, where H_{fs} is the height of the free stream portion of the domain. The computational domain over which the flow is being solved via DNS includes a free stream of height H_{fs} and a portion of the subsurface of depth H_{sub} (Fig. 1). The depth of the subsurface ($H_{sub}/H_{fs} = 0.6$) is sufficient to reach steady Darcy flow beneath the turbulent free stream in the flow calculation. Therefore $z = -H_{sub}$ is merely a computational boundary for the flow solver, and the flow is assumed to be steady and uniform beneath this depth. At the top boundary, $z = H_{fs}$, a free-slip boundary condition is applied, and a fixed pressure gradient is used to drive flow in the x direction. The lateral boundaries are assumed periodic. At the bottom boundary of the flow computational domain a free-slip boundary condition is imposed, with steady Darcy flow assumed beneath the computational domain. Time integration is performed using a third-order Runge-Kutta (RK3) scheme. What results is a three-dimensional, time-dependent, turbulent velocity field that is fully resolved in the free stream and gradually transitions to steady Darcy flow deep in the subsurface – see Fig. 1. In the following analysis, velocities are nondimensionalized by the friction velocity $u_* = \sqrt{\tau_w/\rho}$ (where τ_w is the total surface stress felt by the free-stream), lengths are nondimensionalized by H_{fs}, and time is nondimensionalized by $t^* = H_{fs}/u_*$. Note that free stream refers to flow above the SWI.

This Eulerian velocity field is used to transport random walk particles which each travel with the local fluid velocity and experience constant dispersion via Brownian motion,

$$\mathbf{x}_p(t + \Delta t) = \mathbf{x}_p(t) + \mathbf{u}(\mathbf{x}_p, t)\Delta t + \xi\sqrt{2D_m\Delta t}, \tag{4}$$

where $\mathbf{u}(\mathbf{x}_p, t)$ is the Eulerian (turbulent) fluid velocity interpolated to the particle location $\mathbf{x}_p$, ξ is a normally distributed random variable with mean 0 and unit variance, $\Delta t = 8 \times 10^{-4}$ is the (nondimensional) uniform time step size, and $D_m = 10^{-3}$ is the nondimensional, uniform dispersion coefficient. Note that D_m is *not* meant to represent turbulent

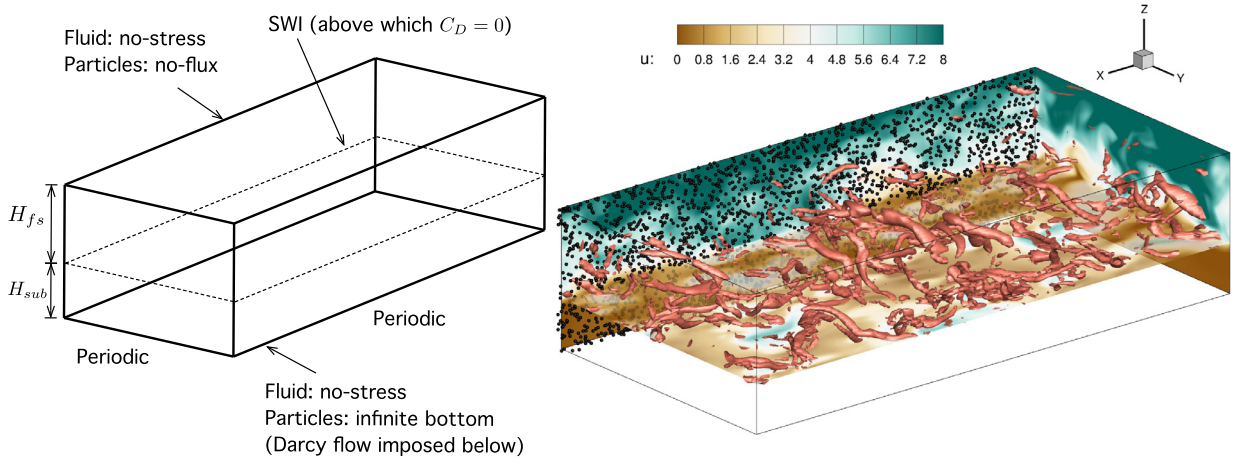

Fig. 1. Left: A schematic of the DNS domain with indications of the various boundary conditions. Dotted lines refer to the SWI. The code solves for the flow in the enclosed box, and Darcy flow is assumed beneath, where the particles experience an infinite bed. Right: An instantaneous snapshot of the DNS solution at $t/t^* = 1.3 \times 10^5$ for the $C_D = 10$, $Re_K = 300$ case. Color contours indicate streamwise velocity magnitude and isosurfaces reflect rotational motions via the swirling strength. Particles are represented as black dots along a representative plane.

dispersion — turbulence is resolved explicitly in the 3D model. In the surface flow, particle transport is dominated by turbulent motion and the influence of D_m is negligible, and thus our use of a uniform D_m is effectively only active in the subsurface. Turbulence strength decreases in the sediment bed and D_m plays an important role in transporting particles vertically through the subsurface. Eq. 4 is solved at the end of each full RK3 step of the DNS. At the top boundary, the Lagrangian particles are reflected to impose a no-flux condition. At the bottom of the computational domain, $z = -H_{sub}$, the particles are free to leave the domain (i.e. they experience an infinitely deep bed), and an advection velocity of $\mathbf{u} = [u_{sub}, 0, 0]$ is imposed reflecting the steady Darcy flow deep in the subsurface. Here, u_{sub} is the steady velocity found at the bottom of the Eulerian computational domain, which reflects the balance between the imposed resistance and the pressure gradient found by solving Eqs. 1 and 2. The underlying bed is considered infinitely deep with a uniform Darcy velocity for the purpose of advecting Lagrangian particles beneath the Eulerian domain. As noted above, the dispersion D_m is meant to reflect a constant background dispersion (either molecular or mechanical), since turbulent transport is explicitly resolved as unsteady advection of the particles. Additional details on the combined Eulerian/Lagrangian computational model can be found elsewhere (Richter and Sullivan, 2013; Sweet et al., 2018).

As detailed below, two primary cases are considered with varying sediment permeability: (1) $C_D = 10$, which corresponds to a free stream Reynolds number of 2500 based on the maximum free stream velocity, the stream height H_{fs}, and the fluid viscosity ν, and (2) $C_D = 100$, which corresponds to a free stream Reynolds number of 3500. Similarly we find the permeability Reynolds number based on the effective permeability of the bed k (calculated assuming Darcy flow deep in the bed, i.e. $u_{sub} = -k\frac{dp}{dx}$) and the friction velocity u_* to be $Re_k \equiv \sqrt{k}u_*/\nu = 300,\ 165$ for $C_D = 10,\ 100$ cases. This ensures that exchange at the SWI is dominated by turbulent motions, as opposed to mechanical dispersion (Voermans et al., 2017). In each case, a total particle number of $N_p = 10^5$ is used and the simulations are advanced for 3×10^6 time steps. Statistics are taken only after a stationary turbulent flow field is developed, and all particles are initialized at the same time and same location $\mathbf{x}_p(t = 0) = [0, \gamma, 0]$, where γ is a uniformly distributed random number spanning the domain in the y direction. At each time step, surface particle concentration at $x = \chi$ is found by counting the number of particles in the surface located in a window, $[\chi - dL, \chi + dL]$ with $dL = 0.1H_{fs}$. These particle concentration histories at fixed observation location are BTCs.

2.2. 2D: Particle tracking model

Using the turbulent velocity field that is fully resolved we obtain a statistically steady velocity field from which a mean velocity profile $\overline{u}(z)$ and a scalar diffusivity profile $\overline{K}(z)$ can be obtained. The scalar diffusivity is calculated directly from the scalar flux and mean scalar gradient in the DNS: $\overline{K}(z) = -\frac{\overline{w'c'}}{\partial_z \overline{C}}$, where c' and $\overline{C}$ are the fluctuating and average scalar concentrations and w' is the fluctuation of the z velocity component in the DNS. Here, overbars refer to averaging in both the horizontal directions (x and y) and in time and fluctuations from this average are denoted with primes. These spatio-temporally averaged profiles are used to parameterize a 2D particle tracking model. As with the DNS, solute is conceptualized as a collection of point particles. Particle i at time t follows a trajectory given by the following Langevin equation (Delay et al., 2005; Kinzelbach, 1988; Noetinger et al., 2016):

$$\begin{aligned} x_i(t + \Delta t) &= x_i(t) + \overline{u}(z_i)\Delta t + \xi_i\sqrt{2D_m\Delta t} \\ z_i(t + \Delta t) &= z_i(t) + \partial_z\overline{K}(z_i)\Delta t + \eta_i\sqrt{2(D_m + \overline{K}(z_i))\Delta t} \end{aligned} \tag{5}$$

Here x_i and z_i are the longitudinal and vertical positions, and ξ_i and η_i are independent and identically distributed random values sampled from a standard normal distribution. Note the term $\partial_z\overline{K}(z_i)\Delta t$ corrects for vertical transport induced by spatial variations in diffusivity and prevents mass-balance discrepancies that would otherwise arise from sharp diffusivity contrasts (see (Delay et al., 2005), equation 40 for more details). No-flux boundary conditions are enforced by elastic reflection at the top boundary, i.e. when a particle crosses the top boundary with position $(x, z + \Delta z)$ it is re-positioned into the computational domain at $(x, z - \Delta z)$. At depths beyond the bottom of the DNS computational domain ($-H_{sub}$), $\overline{K} = 0$ and $\overline{u}(z) = u_{sub}$, the DNS Darcy velocity. Consistent with the DNS, $\Delta t = 8 \times 10^{-4}$ and $D_m = 10^{-3}$. At each model iteration, we find the particle concentration at $x = \chi$ by counting the number of particles in the surface located in a window, $[\chi - dL, \chi + dL]$ with $dL = 0.1H_{fs}$. Counting particles in a window is done to be consistent with how BTCs are calcualted in the DNS.

2.3. 1D ddc-CTRW

In a CTRW framework, particle trajectories are sampled from a travel time/distance pdf $\Psi(l, \tau)$; typically the CTRW is simplified by decoupling time and distance (Berkowitz et al., 2006). The CTRW framework

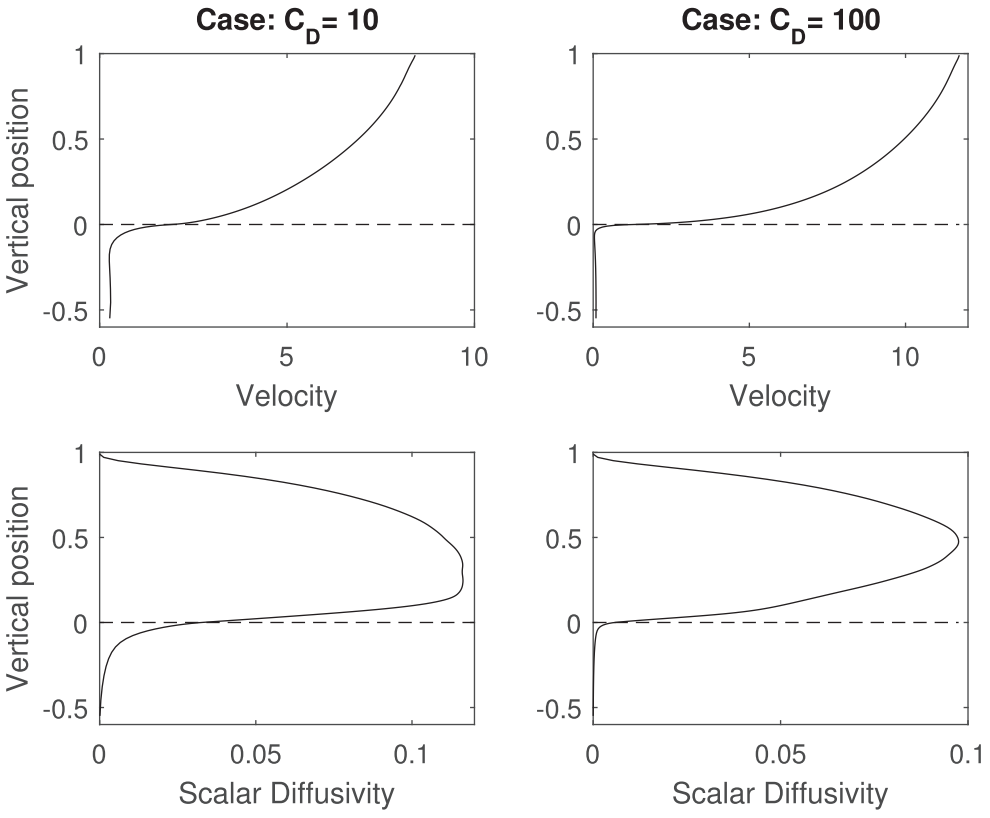

Fig. 2. The DNS spatio-temporally averaged velocity and scalar diffusivity profiles are given for two bed drag coefficients, C_D = 10 (left) and C_D = 100 (right); units are dimensionless. The dashed line indicates the sediment-water-interface. These profiles are input parameters for the 2D particle tracking transport model, which is used to calculate joint PDFs of particle excursions.

has been particularly successful for predicting transport through geologic formations and other porous media. However, such an approach may be limited for the open channel and hyporheic exchange systems under consideration here because treating the entire surface-subsurface continuum with a single distribution makes it impossible to distinguish whether particles cross a control plane in the surface or subsurface as no information related to a particle's transverse position is predicted. To overcome these challenges we introduce a ddc-CTRW.

In the ddc-CTRW, we conceptualize a particle's trajectory as a series of jumps alternating between the subsurface and surface, i.e. after each jump the particle exchanges between the surface and subsurface compartments with probability 1. This reflects the fact that a jump encompasses a particle's entire trajectory between successive exchange events. In each jump particles traverse a distance l in time τ, which are coupled and probabilistically sampled from a joint pdf. Let $\psi_w(l, \tau)$ and $\psi_s(l, \tau)$ be the surface and subsurface time-distance joint pdfs, respectively. Then $\psi_D(l, \tau)$ is the set including the joint pdfs for both the surface and subsurface $\psi_D(l,\tau) = \{\psi_w(l,\tau), \psi_s(l,\tau)\}$. ψ_D is the only input parameter required to run the ddc-CTRW. In this study we construct ψ_D by tracking the traverse time and distance of each particle between exchange events in the particle tracking simulations. An exchange event occurs when a particle crosses the SWI. We refer to a particle's entire trajectory between exchange events as an excursion. The 2D and DNS particle tracking simulations described in the previous section allow for separate estimations of ψ_D, which enables us to observe the influence of short time-scale coherent turbulence structures on the joint pdfs. Finding the joint pdfs using the 2D model offers a significant computational advantage when compared with the DNS.

Again we discretize a solute plume into a large number of particles ($N_p = 10^5$). The trajectory of particle i on the $n+1$ model step follows a Langevin equation:

$$x_i^{n+1} = x_i^n + l_D^{n+1} \tag{6}$$

$$t_i^{n+1} = t_i^n + \tau_D^{n+1} \tag{7}$$

We denote x_i^n, t_i^n as a particle's position and its cumulative travel time at the n^{th} model step. During each model step, a particle travels a distance l in time τ, randomly sampled from a corresponding joint pdf. The distribution that is sampled alternates between ψ_w and ψ_s to represent hyporheic exchange, e.g. the $n+1$ model step must sample from ψ_w if model step n sampled from ψ_s and vice versa.

Consistent with the DNS, particles at $t = 0$ are released at the SWI $x = 0$. For simplicity, we assume that diffusion and dispersion transport an equal number of particles to the surface and subsurface during the first model step, i.e. there is a 50-50 split of particles in each surface-subsurface compartment. However, the ddc-CTRW first step assumption can easily be relaxed to fit any initial condition. DNS simulations show that the 50-50 assumption is not correct because the resistance of the subsurface bed preferentially directs particles to the surface at the first step ($\sim$60% of particles enter the surface for both drag coefficients) because $\partial_z \overline{K}(z_i)$ is positive at the SWI. However we also tested an initial condition that matches the DNS surface-subsurface mass distribution at the first model step, and found that this initial condition only affected the surface-subsurface mass distribution at early times and not downstream transport, i.e. BTCs.

At each model step, we store a particle's position, total travel time, and the traverse time and distance of its previous excursion. This framework enables prediction of BTCs at downstream position χ. Let f be the first model step such that particle i's cumulative travel time exceeds a time t. Then, using linear interpolation, the particle's position at time t is $x_i^f - (t_i^f - t)\frac{l^f}{\tau_i^f}$. A BTC at position χ is constructed by counting the number of particles in window $[\chi - dL, \chi + dL]$ at each time t.

3. Results and discussion

3.1. Effects of drag coefficients on mean profiles

Two different sediment bed drag coefficients are considered in the DNS framework, $C_D = 10$ and $C_D = 100$, resulting in the ratio of mean

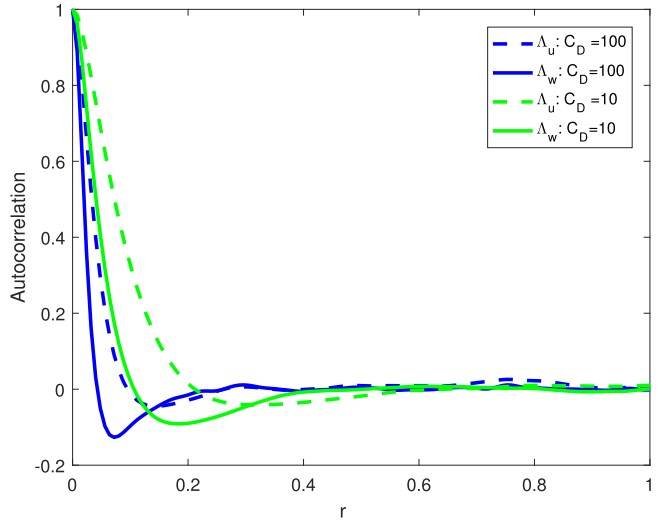

Fig. 3. Velocity fluctuation time autocorrelations measured at the SWI for both streamwise and vertical directions: $\Lambda_u(r) = \overline{u'(t)u'(t+r)}/\overline{u'^2}(z=0)$ and $\Lambda_w(r) = \overline{w'(t)w'(t+r)}/\overline{w'^2}(z=0)$, where r denotes the dimensionless time delay.

channel to mean subsurface velocity being approximately 20 and 90 respectively. These ratios are consistent with BTCs measured from pulse experiments in streams with cobble and pea gravel substrates (Aubeneau et al., 2016), where the surface to subsurface velocity ratio (approximately equal to the ratio of latest arrival time to arrival of peak concentration) ranged from $O(10) - O(100)$. The effective permeability of the subsurface in the low drag case is 3.2 times greater than the high drag case. The lower permeability bed of the $C_D = 100$ case more rapidly removes turbulent momentum from the flow, thereby causing a more rapid decay of mean streamwise velocity and scalar diffusivity with increasing depth in the streambed (Fig. 2). The non-Darcy velocity portion of the bed experiences increased turbulence in the $C_D = 10$ case, demonstrated by a permeability Reynolds number $Re_k = 300$ vs. $Re_k = 165$ for the high drag case. Note that bed turbulence is significantly weaker than in the free stream, where the Reynolds numbers are approximately an order of magnitude larger.

The DNS snapshot (Fig. 1) illustrates the presence of coherent structures near the bed, as given by local rotation of the fluid motion. These structures enable rapid transport across the SWI, and in the mean sense are responsible for the turbulent flux of scalar $\overline{w'c'}$. Naturally, the structures are only temporary as the turbulent flow is constantly evolving. Such coherent, 3D motions are inherently absent in the 2D model as the scalar diffusivity parameter represents the time average of turbulent fluctuations in scalar concentration. As such, the 2D (and therefore 1D) model is unable to accurately represent scalar transport at timescales shorter than the characteristic lifetime of these structures. The timescale in which coherent turbulent structures dictate particle motions is estimated by calculating the autocorrelation of velocity fluctuations at the SWI (Fig. 3). Velocity fluctuations become uncorrelated at roughly 0.7 and 0.35 nondimensional times for the $C_D = 10,\ 100$ cases. Hence for a stream with a depth of O(10 cm) and u_* of O(1 cm/s) as observed in Packman and MacKay (2003), the lifetime of a turbulent structure is only of order 1-10s. Structures in the $C_D = 10$ case have longer lifetimes near the SWI due to the smaller bed resistance. The 2D model is only valid when averaged over many coherent motions, at which time the motion becomes decorrelated.

3.2. DNS Vs 2D particle tracking model

3.2.1. Joint PDFs: Particle trajectory comparison

We observe the influence of coherent turbulent structures on particle excursions by comparing the travel time/distance joint pdfs from the

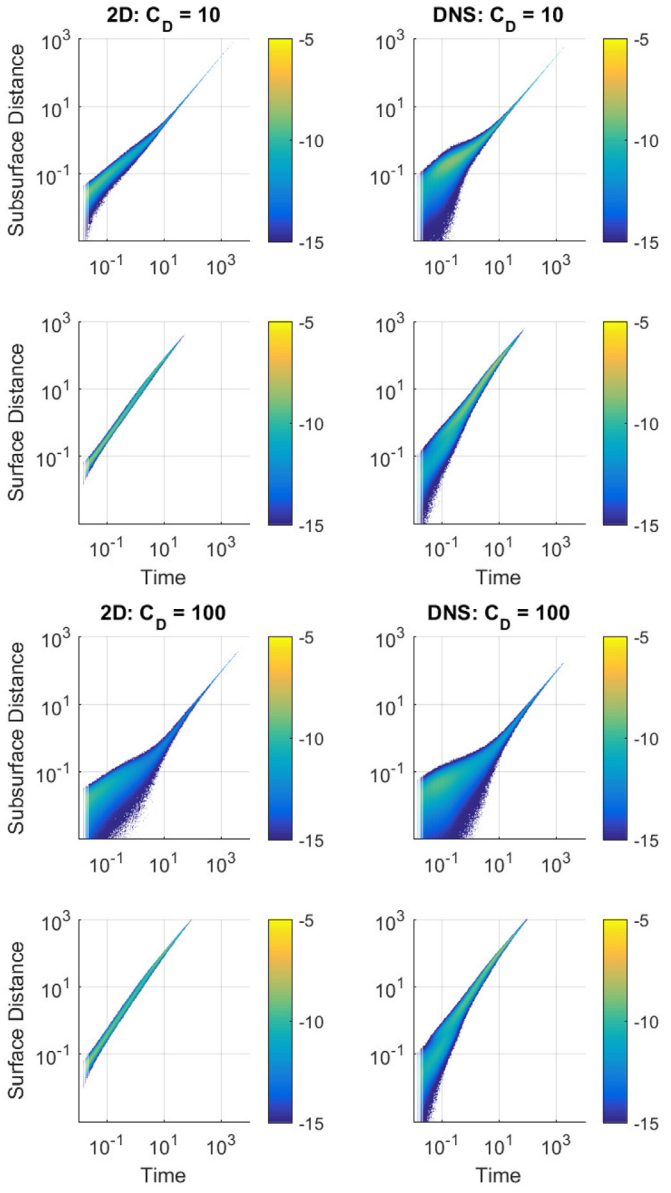

Fig. 4. A comparison of surface and subsurface joint pdfs for the 2D particle tracking model with measurements from DNS. Time and streamwise distances are given in dimensionless units. The colorbar shows log of probability. (For interpretation of the references to color in this figure legend, the reader is referred to the web version of this article.)

DNS and 2D model. These are computed in both models by calculating the time and streamwise distance traveled by each particle during each surface or subsurface excursion. The general shape of both the surface and subsurface 2D joint pdfs match well with the DNS pdfs for each drag case (Fig. 4). Differences between models are most pronounced for particle excursions less than the time scale of velocity decorrelation, seen as a widening of the distribution in distance for a corresponding travel time in the DNS. As excursion travel time increases, trajectories asymptotically approach a corresponding distance governed by an effective velocity. This is clearly evident in all subsurface PDFs, where particles can remain in the turbulence-free portion of the subsurface for long times and motion is dominated by the mean Darcy velocity. In the surface flow, the range of travel distances at large times ($t > 1$) is greater than in the subsurface because both channel turbulence and the average velocity is substantially stronger in the surface, – e.g. at $t = 1$ in the $C_D = 10$ case, travel distances range from 1.4 to 7.7 in the surface while

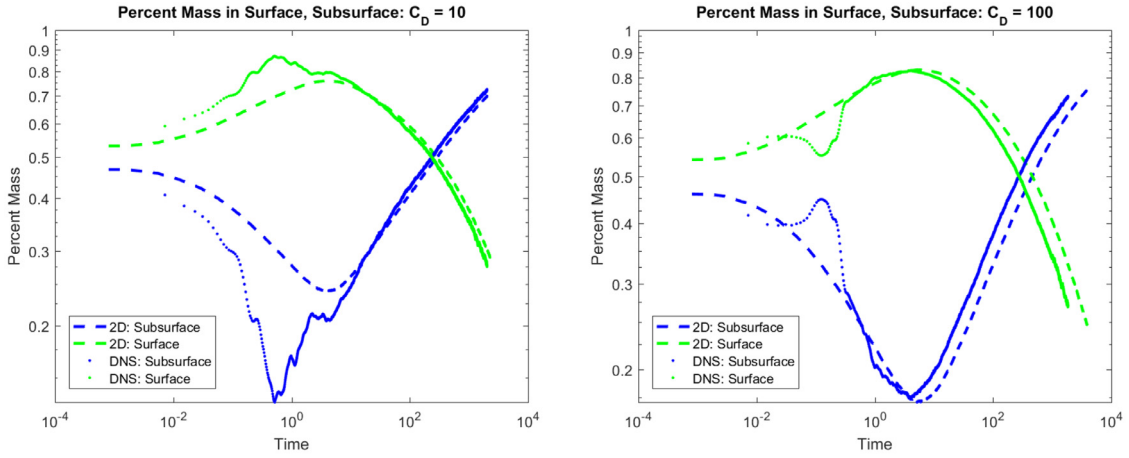

Fig. 5. The percent of particles in surface and subsurface at each time step in the 2D particle tracking model and DNS for two drag cases.

subsurface distances range from only 0.08 to 1. Coherent turbulent dispersive effects begin to average to a mean dispersion as distance from the particle source increases and so particle transport begins to resemble transport governed by the mean velocity field and mean turbulent dispersion profile.

In both domains of the DNS and 2D model, turbulent coherent structures have a greater relative impact on particle excursions at early times because particles do not have ample time to sample the flow field. These coherent structures present in the DNS, but not in the 2D model due to averaging, cause a wider distribution in travel distance for all timescales in the DNS. This is especially noticeable in the surface where turbulence is stronger. Despite neglecting these structures, the 2D model and DNS excursion distributions share a similar shape, meaning the ddc-CTRW can be accurately parameterized with the 2D model.

3.2.2. Hyporheic exchange comparison

We observe hyporheic exchange by measuring the percent of particles in both the surface and subsurface domain over time for the DNS and 2D model (Fig. 5). The 2D model does not agree with the DNS at short times ($t<1$) because short-time transport is controlled by turbulent coherent structures in the DNS. Particles carried by these structures are correlated until approximately one non-dimensional time scale $t\sim t^*$, and these correlations violate the underlying description of particle motion in the 2D model (Eq. 5). The decreased (increased) percent subsurface mass at early times is attributed to local turbulent coherent structures sweeping particles out of (into) the subsurface for the $C_D = 10$ ($C_D = 100$) case. The location and timing of specific sweeping events varies by DNS realization, so early behavior in percent surface mass (Fig. 5) is highly dependent on the time and location of initial particle release. Note that due to computational constraints we only conduct one DNS realization.

As time increases in both models, the total mass in the surface decreases because the infinite bed allows particles to reside in the subsurface for long durations. The Taylor dispersion timescale, the characteristic time for a solute to fully sample the velocity field, is defined as $\tau_T = a^2/D_T$, where a is a characteristic length scale and D_T is the dispersion coefficient. We calculate D_T as the vertically averaged surface dispersion from the 2D model and a as the channel depth H_{fs}; $\tau_T = 11.1,\ 24.9$ in the surface for the $C_D = 10,\ 100$ cases, respectively. At times greater than τ_T the mass transfer rates across the SWI in the two models are consistent, demonstrated by the nearly identical slopes of percent mass over time (Fig. 5). Thus after a sufficient time, approximately equal to a Taylor timescale, the hyporheic exchange rate in the DNS can be accurately estimated with mean scalar diffusivity and velocity profiles.

3.3. ddc-CTRW Breakthrough Curve Predictions

For both the DNS and 2D pdf inputs the predicted BTCs from the ddc-CTRW closely match the DNS BTCs (Fig. 6), especially as distance from the particle source increases. This convergence is expected because as downstream distance increases, particles have more time to sample the velocity field resulting in motion that closely resembles one governed by mean velocity and scalar diffusivity profiles. As distance from the source increases, single coherent turbulent structures have a reduced impact on macro-scale transport because their effects are averaged out.

We compare BTC agreement by calculating the first, second, and third, centered temporal moments, representing the mean arrival, the variance, and skewness, respectively (Fig. 7). The first temporal moment is calculated as $M_1 = \int_\infty^\infty tC(t)dt$ and the *ith* centered moment is defined as $M_i = \int_\infty^\infty (t-M_1)^i C(t)dt$ for $i>1$. There is excellent agreement of moments at far downstream locations and greater deviation near the location of initial particle release. Note that BTCs from the ddc-CTRW and the 2D model are nearly identical (results not shown). This suggests that at a sufficiently large distance from the solute source, the 2D model and ddc-CTRW both accurately represent the distribution of arrival times calculated in the DNS.

A normalized mean squared error (MSE) is calculated between ddc-CTRW BTC predictions and DNS simulations at control plane j as $MSE = \frac{1}{A_{BTC_j} N}\sum_{i=1}^{N}(C(t_i)_{DNS} - C(t_i)_{ddc-CTRW})^2$, where A_{BTC_j} is the area under the BTC at control plane j, N is the number of DNS time steps and $C(t_i)$ is the particle concentration at time step i calculated from simulated BTCs. The greatest MSE occurs at the first two control plane locations, $x = 12.6$ and $x = 23.1$ (Fig. 8). Predicted peak concentration also shows the most significant deviation from the DNS at these control planes. We find a characteristic length scale L_T where sufficient statistical sampling will have occurred for an ensemble representation to hold by multiplying the Taylor timescale by a mean velocity. We define $L_w = \overline{\overline{u_w}} H_{fs}^2/\overline{\overline{K_w}}$ as the distance at which particles have fully sampled the surface velocity distribution, where $\overline{\overline{u_w}}$ is the vertically averaged mean surface velocity and $\overline{\overline{K_w}}$ is the vertically averaged mean surface scalar diffusivity. In our simulations, $L_w = 61,\ 128$ for the $C_D = 10,\ 100$ cases respectively, corresponding to where the rate of decrease in MSE with distance begins to temper.

In both drag cases, particle concentration near the BTC peak is approximately equal between the ddc-CTRW and DNS models at distances exceeding $x = 78$, similar to what is expected from the characteristic length L_w (Fig. 6). The shape of BTCs near peak concentration is dominated by surface flow, where as BTC power-law tailing is dominated by particles being retained in the slower moving subsurface. We

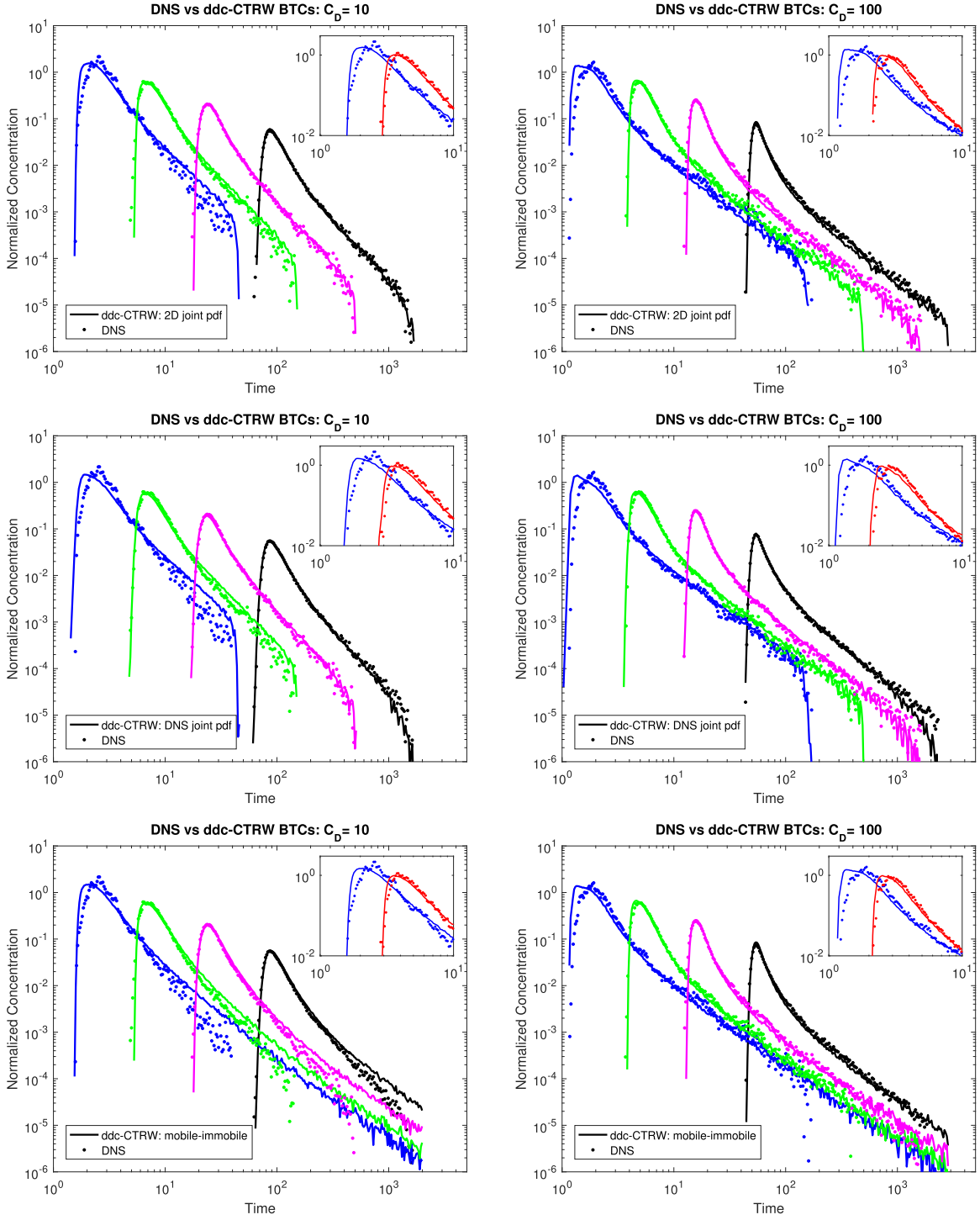

Fig. 6. Measured and predicted breakthrough curves are shown at 12, 42, 143 and 483 dimensionless lengths from the solute source. Inset: BTC peak arrival at 12 and 23 lengths from the solute source, showing predicted BTCs with the greatest deviation from DNS. The left and right columns correspond to sediment bed drag coefficients of 10 and 100, respectively. The first row is a comparison between the ddc-CTRW parameterized from the 2D particle tracking model pdfs with DNS simulations. The second row shows predictions from the ddc-CTRW parameterized with DNS pdfs. The third row gives model predictions of a mobile-immobile CTRW parameterized with the 2D model pdfs: subsurfac travel distances are neglected.

find an additional Taylor-like length scale over the entire water column and the portion of the bed penetrated by turbulence ($H_{fs} + H_{sub}$) as $L_{SH} = 147,307$ for the $C_D = 10,\ 100$ cases, respectively. The model agreement for tailing of the ddc-CTRW with the DNS occurs at close proximity to these estimated length scales. At distances less than these lengths, the ddc-CTRW model overpredicts concentrations in power-law tails because the particle excursion distributions have not yet converged to the input pdf parameters.

3.3.1. *ddc-CTRW Sensitivity to Subsurface Travel Distances*

To test the sensitivity of model outputs to subsurface travel distances, we rerun the ddc-CTRW with a mean subsurface velocity. That is, we

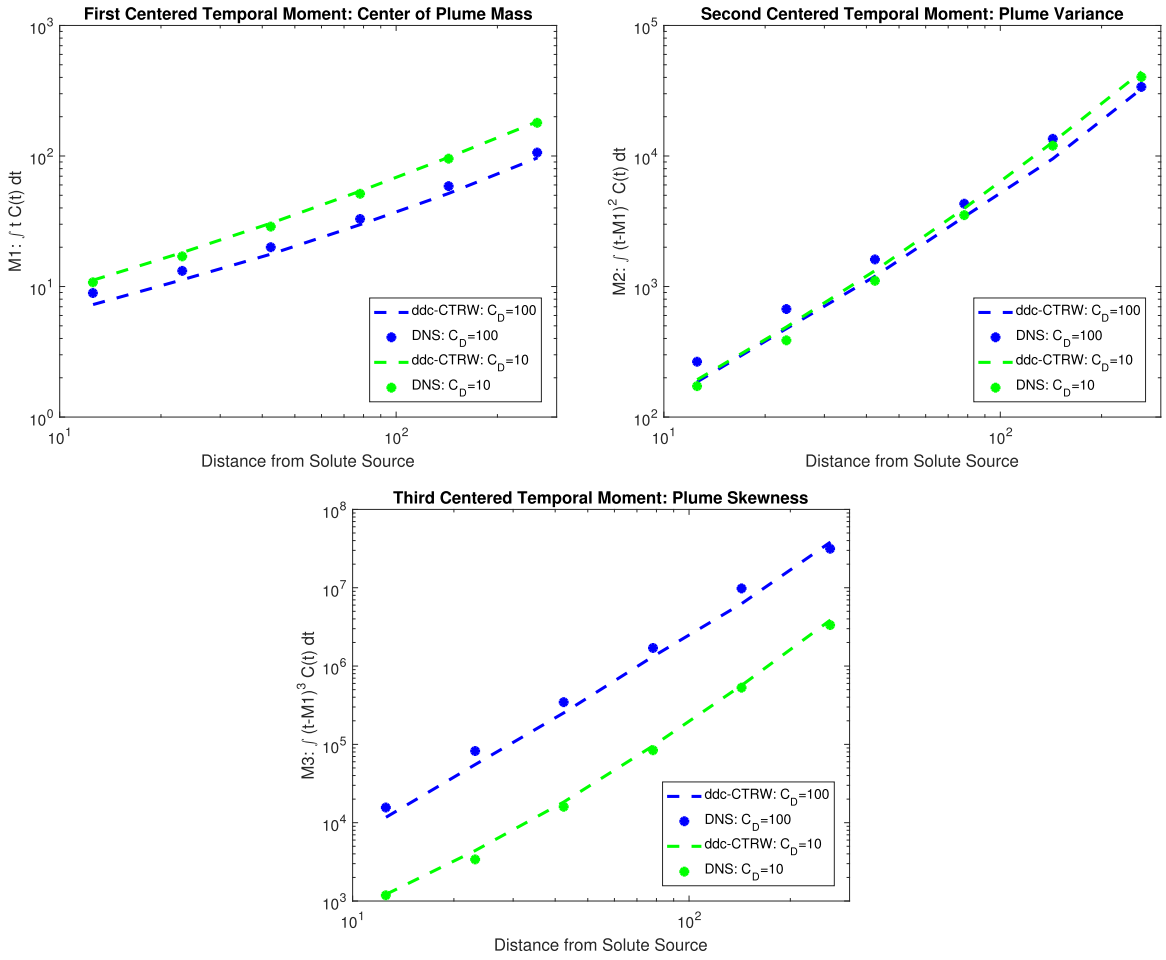

Fig. 7. A comparison of the first, second, and third temporal moments measured in the DNS and a ddc-CTRW parameterized with the 2D model pdfs for two drag coefficients.

again parameterize the ddc-CTRW with the surface travel time/distance pdf, but now only sample a subsurface travel time with a corresponding distance calculated as the selected time multiplied by the mean subsurface velocity, u_{sub}. In this parameterization scheme, there is virtually no difference in predicted BTCs from the mean subsurface ddc-CTRW with the ddc-CTRW parameterized with the 2D model pdfs (Fig. 9). In our systems this agreement is expected because travel distances are negligible at small subsurface residence times and particle travel velocity asymptotically approaches the mean subsurface velocity with increasing excursion time (Fig. 4). The increased range in surface travel distances at large times makes the analogous argument invalid for the surface case, as the finite depth of the channel makes it nearly impossible for particles to remain in the surface long enough to all approach the same mean velocity.

Furthermore, we test a CTRW framework where particles sample the same surface and subsurface travel times as the ddc-CTRW, but now particles all travel according to a mean surface and mean subsurface velocity for the respective domains. The mean surface velocity is the vertically averaged channel velocity ($\bar{\bar{u}} = \frac{1}{H_{fs}} \int_0^{H_{fs}} \bar{u}(z) dz$) and the subsurface velocity is again the Darcy velocity. The dashed lines in Fig. 9 show BTC predictions with this framework. The BTC peak is the area most affected by the surface flow. Neglecting surface velocity variations reduces the range of possible particle trajectories, which manifests as a narrowing of BTC peak widths. Enforcing a mean velocity also prevents particles from persisting in the fastest velocities of the flow, and so the earliest arrival times are delayed. The turbulent nature of the surface flow suggests transverse velocity variations should be considered in a 1D-framework for accurate representation of BTC peak concentration at the scales of interest considered in this study.

We also predict BTCs with a mobile-immobile CTRW that neglects travel distances in the subsurface (Fig. 6: bottom row), an assumption consistent with the framework most typically applied to date Boano et al., 2007. In this model, surface trajectories and subsurface travel times are identical to those used in the ddc-CTRW model based on the DNS simulation, but subsurface particle travel distances are set to zero so that particles in the subsurface do not advect downstream. This model also effectively captures breakthrough of peak concentrations, as particle trajectories with these arrival times are dominated by the surface flow field. In contrast, late-time tailing is drastically overestimated because mass cannot cross BTC control planes while in the subsurface, manifesting as late-time breakthrough which otherwise would have occurred in the subsurface (Roche et al., 2017). In the DNS, breakthrough curves truncate at approximately χ/u_{sub}, where χ is the downstream position and u_{sub} is the Darcy velocity. This truncation is captured when subsurface velocity is incorporated into the CTRW framework, as done in the ddc-CTRW. These results demonstrate that when the ratio of surface to subsurface velocity is low (i.e. $O(10)$ or less), subsurface velocities may significantly impact late-time arrival. As both the distance from the source and the surface to subsurface velocity ratio increase, treating the subsurface as an immobile zone becomes more reasonable. In the $C_D = 100$ case, when the surface to subsurface velocity ratio is $O(100)$, this mobile-immobile CTRW accurately predicts BTCs at the farthest distances considered in our simulations. Hence, subsurface advection should be accounted for at the lengths scales considered in this study,

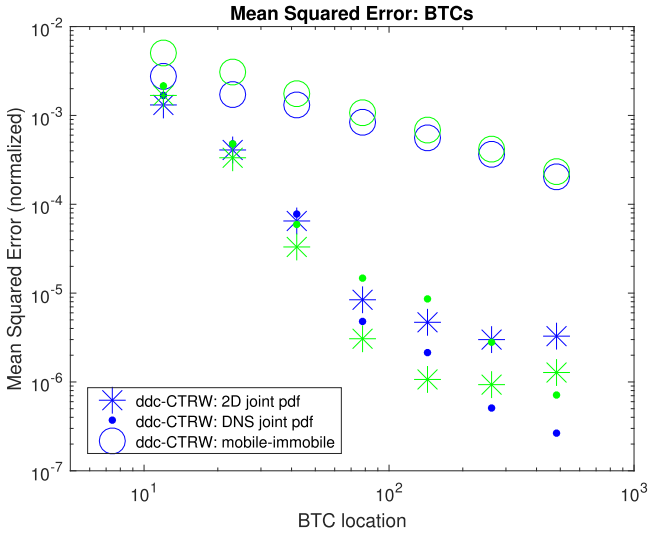

Fig. 8. The normalized mean squared error (MSE) is calculated between ddc-CTRW BTC predictions and the DNS at control plane j as $MSE = \frac{1}{A_{BTC_j} N} \sum_{i=1}^{N} (C(t_i)_{DNS} - C(t_i)_{ddc-CTRW})^2$, where A_{BTC_j} is the area of the BTC at control plane j, N is the number of DNS time steps and $C(t_i)$ is the particle concentration at time step i. The MSE for the ddc-CTRW parameterized with DNS pdfs (stars), the ddc-CTRW parameterized with the 2D model pdfs (dots), and the mobile-immobile ddc-CTRW (circle) is provided for the $C_D = 10$ (green) and $C_D = 100$ (blue) case. BTC locations correspond to distances 12, 23, 42, 78, 143, 263 and 483 dimensionless lengths from the solute source, respectively. (For interpretation of the references to color in this figure legend, the reader is referred to the web version of this article.)

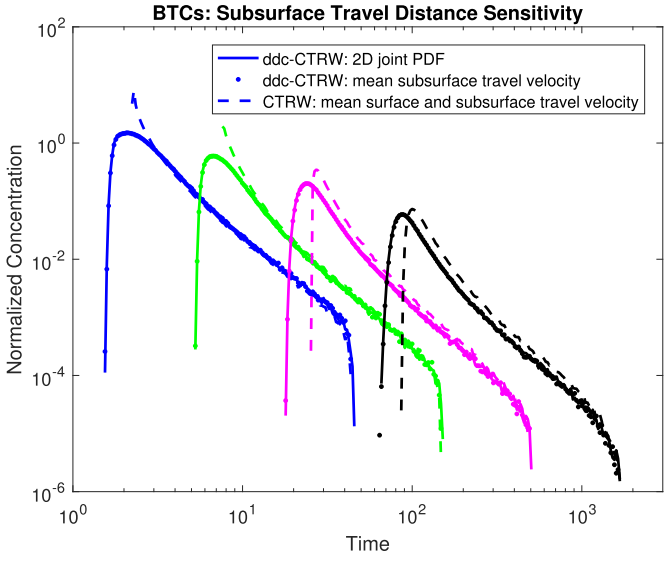

Fig. 9. A comparison of predicted BTCs with different ddc-CTRW frameworks. Solid lines are predictions from a ddc-CTRW which samples from the complete 2D C_D=10 joint pdfs in both the surface an subsurface. Dots are predictions from a ddc-CTRW that samples from the 2D C_D=10 surface pdf, and travels according to a mean velocity in the subsurface; note predictions are nearly identical to the full ddc-CTRW framework. Dashed lines are predictions from a ddc-CTRW where particles travel according to a mean surface and mean subsurface velocity.

when the surface to subsurface velocity ratio is less than $O(100)$. Additionally, as the distance from the particle source increases the surface BTC truncation time also increases and therefore considering the subsurface as entirely immobile becomes a more reasonable assumption.

Subsurface travel distances may be neglected as the ratio of surface to subsurface velocity increases because surface flow plays an increasing

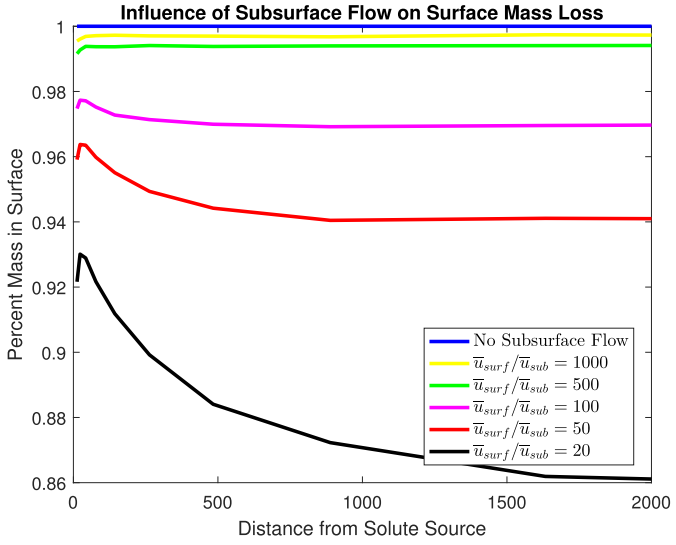

Fig. 10. The ddc-CTRW is applied with a constant subsurface velocity. We show percent of initial mass that crosses BTC control planes in the surface for different ratios of mean surface velocity to subsurface velocity. As this ratio decreases, mass lost to the subsurface become significant.

role in streamwise transport. We apply our ddc-CTRW to investigate the effect of subsurface velocity on apparent surface BTC mass loss by measuring the percent of injected particles that crosses in the surface at each BTC plane for different ratios of mean surface to subsurface velocities (Fig. 10). In this analysis, the ddc-CTRW inputs are the $C_D = 10$ surface joint pdf and the $C_D = 10$ travel time pdf with distances found using the mean velocity method described previously. When the surface to subsurface mean velocity ratio exceeds 500, less than 2% of mass propagates past BTC control planes in the subsurface at downstream distances surpassing 1000 non-dimensional lengths. However at a ratio of 20, 7.5 times as many particles ($\sim$15%) cross the BTC control plane while in the subsurface at the same distance. Incorporating subsurface trajectories into a modeling framework becomes increasingly important as subsurface velocities increase, which increases with bed permeability and the hydraulic gradient. A benefit of this proposed ddc-CTRW is that it generalizes previous frameworks and can easily reduce to a mobile-immobile model.

3.4. Computational benefits and limitations

Upscaled modeling frameworks provide an obvious computational advantage over DNS because they do not resolve all scales of turbulent motion. We compare computational cost by cpu hours, the total time to complete a simulation multiplied by the number of cores. In this study, the DNS run time using 10^5 particles was $O(10, 000)$ cpu hours which took weeks to complete using a 64-core (Intel Ivy Bridge) computational cluster. The corresponding 2D simulation run time was $O(10)$ cpu hours and the corresponding ddc-CTRW run time was $O(0.01)$ cpu hours. However, both the 2D model and ddc-CTRW require model input parameters which are directly or indirectly calculated from the DNS. Therefore, the full reduction in computational cost offered by the ddc-CTRW is only truly achieved if input parameters are known *a priori* to DNS. Note that the mean DNS velocity and scalar diffusivity profiles converge after $O(1, 000)$ cpu hours.

This drastic reduction in run time demonstrates the potential benefits of the ddc-CTRW framework, but estimating input parameters without relying on higher dimensional particle tracking simulations remains an open question. One possible method for parameterizing the subsurface joint pdf is to estimate subsurface residence time with a truncated power law distribution (Boano et al., 2007) and then advect particles with a

Darcy velocity. A paramterization scheme such as a noise-driven mass balance model (Aquino et al., 2017) may be better suited to estimate the surface joint pdf because it captures surface velocity fluctuations, which are important for capturing peak BTC concentration. Paramterizing the ddc-CTRW with these methods remain untested and warrants further investigation.

Even without *a priori* knowledge of model input parameters, the ddc-CTRW still offers a significant computational advantage over DNS because the input travel time/distance joint pdfs can be calculated prior to completion of a full DNS run. Since the mean DNS velocity and scalar diffusivity profiles converge after $O(1,\ 000)$ cpu hours, only a portion of the DNS needs to be completed to parametrize the 2D model. Given the 2D model is initialized with a large number of particles, we only need to calculate travel time and distance of the first surface and subsurface excursion for each particle to estimate the ddc-CTRW input joint pdfs, meaning that again the 2D model does not need to be run until completion. Thus with this methodology, we can still parameterize the ddc-CTRW and accurately predict DNS BTCs at a significantly reduced computational cost.

As with any successful modeling effort, the system under consideration must satisfy the assumptions embedded into the model framework. The ddc-CTRW assumes that joint pdf input parameters do not change in time and space; i.e. stationary, homogeneous turbulence with a constant channel geometry and permeability. Our idealized river system satisfies these assumptions and therefore produces excellent agreement between ddc-CTRW predictions with DNS BTCs. Given the highly dynamic nature of real streams and rivers coupled with a changing bed geometry, the length and time scales that meet these assumptions must be considered. However, parameterizing such dynamical behavior is a limitation that all current state of the art effective models suffer from. Despite the ddc-CTRW's limitations, it carries obvious computational advantages over turbulence resolving DNS experiments and can help advance the understanding of underlying physical processes controlling transport as they are inferred from BTCs. Specifically a ddc-CTRW framework helps quantify the length scales at which subsurface advection must be accounted for and the evolution of solute in the subsurface through space and time.

4. Conclusions

In this study, we find that the surface and subsurface joint travel time/distance pdfs provide enough information to accurately portray hyporheic exchange and transport in an idealized open channel system. We leverage such data in a ddc-CTRW framework and accurately predict BTCs of the high-fidelity, turbulence-resolving DNS after a sufficient distance, which is defined as a Taylor-like length scale. The ddc-CTRW allows mass to advect downstream while in the subsurface, which has been neglected in most models to date. We find that when the ratio of surface to subsurface velocity is of $\sim O(10)$, subsurface advection must be considered in an upscaled framework to accurately predict BTC tailing behavior. The ddc-CTRW framework is especially advantageous because it reduces to a mobile-immobile CTRW when streamwise subsurface advection is ignored, but by incorporating both subsurface and surface advection it can characterize quantities such as the percent of initial mass in the subsurface at a given location. Such characterization can be important in interpretation and design of experiments where subsurface mass is undetectable in conventional in-stream BTC measurements. Furthermore, the computational cost of the ddc-CTRW is orders of magnitude less than that of a DNS and therefore, the ddc-CTRW is a computationally efficient model which can aid in the understanding of hyporheic exchange and transport in river systems.

Acknowledgments

The authors gratefully acknowledge financial support from NSF via grants EAR 1351625 and CBET 1705770. We thank the University of Notre Dame Center for Research Computing for computational resources and support.

References

Aquino, T., Aubeneau, A., Bolster, D., 2015. Peak and tail scaling of breakthrough curves in hydrologic tracer tests. Adv. Water Resour. 78, 1–8.
Aquino, T., Aubeneau, A., McGrath, G., Bolster, D., Rao, S., 2017. Noise-driven return statistics: scaling and truncation in stochastic storage processes. Sci. Rep. 7 (1).
Aubeneau, A., Hanrahan, B., Bolster, D., Tank, J.L., 2014. Substrate size and heterogeneity control anomalous transport in small streams. Geophys. Res. Lett. 41 (23), 8335–8341.
Aubeneau, A.F., Hanrahan, B., Bolster, D., Tank, J., 2016. Biofilm growth in gravel bed streams controls solute residence time distributions. J. Geophys. Res. 121 (7), 1840–1850.
Battin, T., Kaplan, L., Findlay, S., Hopkinson, C., Mart, E., Packman, A. I., Newbold, D., Sabater, F., 2009. Biophysical controls on organic carbon fluxes in fluvial networks. 1 95–100.
Benson, D.A., Schumer, R., Meerschaert, M.M., Wheatcraft, S.W., 2001. Fractional dispersion, lévy motion, and the MADE tracer tests. In: Dispersion in Heterogeneous Geological Formations, Transport in Porous Media, 42, pp. 211–240.
Berkowitz, B., Cortis, A., Dentz, M., Scher, H., 2006. Modeling non-Fickian transport in geological formations as a continuous time random walk. Rev. Geophys. 44 (2), RG2003.
Berkowitz, B., Scher, H., 2009. Exploring the nature of non-fickian transport in laboratory experiments. Adv. Water Resour. 32 (5), 750–755.
Boano, F., Harvey, J.W., Marion, A., Packman, A.I., Revelli, R., Ridolfi, L., Wrman, A., 2014. Hyporheic flow and transport processes: mechanisms, models, and biogeochemical implications. Rev. Geophys. 52 (4), 603–679.
Boano, F., Packman, A.I., Cortis, A., Revelli, R., Ridolfi, L., 2007. A continuous time random walk approach to the stream transport of solutes. Water Resour. Res. 43 (10).
Bolster, D., Méheust, Y., Borgne, T.L., Bouquain, J., Davy, P., 2014. Modeling preasymptotic transport in flows with significant inertial and trapping effects - the importance of velocity correlations and a spatial Markov model. Adv. Water Resour. 70 (0), 89–103.
Borgne, T.L., Dentz, M., Carrera, J., 2008. Lagrangian statistical model for transport in highly heterogeneous velocity fields. Phys. Rev. Lett. 101 (9), 090601.
Cortis, A., Birkholzer, J., 2008. Continuous time random walk analysis of solute transport in fractured porous media. Water Resour. Res. 44 (6).
Delay, F., Ackerer, P., Danquigny, C., 2005. Simulating solute transport in porous or fractured formations using random walk particle tracking. V top Vadose Zone J. 4, 360–379.
Drummond, J.D., Aubeneau, A.F., Packman, A.I., 2014. Stochastic modeling of fine particulate organic carbon dynamics in rivers. Water Resour. Res. 50.
Finnigan, J.J., Shaw, R.H., Patton, E.G., 2009. Turbulence structure above a vegetation canopy. J. Fluid Mech. 637, 387–424.
González, C., Richter, D.H., Bolster, D., Bateman, S., Calantoni, J., Escauriaza, C., 2017. Characterization of bedload intermittency near the threshold of motion using a lagrangian sediment transport model. Environ. Fluid Mech. 17 (1), 111–137.
González-Pinzón, R., Haggerty, R., Dentz, M., 2013. Scaling and predicting solute transport processes in streams. Water Resour. Res. 49 (7), 4071–4088.
Gooseff, M.N., 2010. Defining hyporheic zones advancing our conceptual and operational definitions of where stream water and groundwater meet. Geogr. Compass 4 (8), 945–955.
Haggerty, R., Fleming, S.W., Meigs, L.C., McKenna, S.A., 2001. Tracer tests in a fractured dolomite: 2. analysis of mass transfer in single-well injection-withdrawal tests. Water Resour. Res. 37 (5), 1129–1142.
Haggerty, R., McKenna, S.A., Meigs, L.C., 2000. On the latetime behavior of tracer test breakthrough curves. Water Resour. Res. 36 (12), 3467–3479.
Haggerty, R., Wondzell, S.M., Johnson, M.A., 2002. Powerlaw residence time distribution in the hyporheic zone of a 2nd order mountain stream. Geophys Res. Lett. 29 (13), 18–1–18–4.
Harvey, J.W., Wagner, B.J., Bencala, K.E., 1996. Evaluating the reliability of the stream tracer approach to characterize streamsubsurface water exchange. Water Resour. Res. 32 (8), 2441–2451.
Kang, P.K., de Anna, P., Nunes, J.P., Bijeljic, B., Blunt, M.J., Juanes, R., 2014. Pore-scale intermittent velocity structure underpinning anomalous transport through 3-d porous media. Geophys. Res. Lett. 41 (17), 6184–6190.
Kinzelbach, W., 1988. The random walk method in pollutant transport simulation. Groundwater flow and quality modelling 227–245.
Li, A., Aubeneau, A.F., Bolster, D., Tank, J.L., Packman, A.I., 2017. Covariation in patterns of turbulencedriven hyporheic flow and denitrification enhances reachscale nitrogen removal. Water Resour. Res. 53.
Noetinger, B., Benoit, D., Russian, A., Borgne, T.L., Delay, F., Dentz, M., De Dreuzy, J., Gouze, P., 2016. Random walk methods for modeling hydrodynamic transport in porous and fractured media from pore to reservoir scale. Transp. Porous Media 115, 345–385.
Packman, A.I., MacKay, J.S., 2003. Interplay of stream-subsurface exchange, clay particle deposition, and streambed evolution. Water Resour. Res. 39 (4). 1097
Park, H.J., O'Keefe, K., Richter, D.H., 2018. Rayleigh-bénard turbulence modified by two-way coupled inertial, nonisothermal particles. Phys. Rev. Fluids 3, 034307.
Richter, D.H., Sullivan, P.P., 2013. Momentum transfer in a turbulent, particle-laden couette flow. Phys. Fluid. 25, 053304.
Roche, K.R., 2017. Transport Processes at the Sediment Water Interface Ph.D. thesis. Northwestern University.
Roche, K.R., Blois, G., Best, J.L., Christensen, K.T., Aubeneau, A.F., Packman, A.I., 2018. Turbulence links momentum and solute exchange in coarsegrained streambeds. Water Resour. Res. 54.

Sherman, T., Fakhari, A., Miller, S., Singha, K., Bolster, D., 2017. Parameterizing the spatial markov model from breakthrough curve data alone. Water Resour. Res. 53 (12), 10888–10898.
Stonedahl, S.H., Harvey, J.W., Detty, J., Aubeneau, A., Packman, A.I., 2012. Physical controls and predictability of stream hyporheic flow evaluated with a multiscale model. Water Resour. Res. 48.
Sweet, J., Richter, D.H., Thain, D., 2018. GPU Acceleration of eulerian-lagrangian-particle-laden turbulent flow simulations. Int. J. Multiphase Flow 99, 437–445.
Taylor, G., 1954. The dispersion of matter in turbulent flow through a pipe. In: Proceedings of the Royal Society of London A: Mathematical, Physical and Engineering Sciences. 223 (1155) 446–468
Voermans, J.J., Ghisalberti, M., Ivey, G.N., 2017. The variation of flow and turbulence across the sediment–water interface. J. Fluid Mech. 824, 413–437.
Voermans, J.J., Ghisalberti, M., Ivey, G.N., 2018. A model for mass transport across the sedimentwater interface. Water Resour. Res. 54 (40), 2799–2812.
Wlostowski, A.N., Gooseff, M.N., Bowden, W.B., Wollheim, W.M., 2016. Stream tracer breakthrough curve decomposition into mass fractions: a simple framework to analyze and compare conservative solute transport processes. Limnol. Oceanogr. Methods 15 (2), 140–153.
Wörman, A., Packman, A.I., Johansson, H., Jonsson, K., 2002. Effect of flowinduced exchange in hyporheic zones on longitudinal transport of solutes in streams and rivers. Water Resour. Res. 38 (1), 2–1–2–15.